Iranian Journal of Materials Forming 8 (1) (2021) 50-64

Online ISSN: 2383-0042

Iranian Journal of Materials Forming

Journal Homepage: http://ijmf.shirazu.ac.ir

Research Article

Vibratory Stress Relief of Welded Austenite Stainless Steel Plates: A Numerical and Experimental Approach

F. Tatar, A.H. Mahmoudi* and A. Shooshtari

Mechanical Engineering Department, Bu-Ali Sina University, Hamedan, Iran

ARTICLE INFO

Article history:

Received 4 August 2020
Reviewed 28 September 2020
Revised 10 November 2020
Accepted 11 December 2020

Keywords:

Vibratory stress relief
Modal analysis
Bead-on-plate welding
ICHD measurement

ABSTRACT

Residual stresses are one of the most important factors in the integrity of welded structures. There have been vast majorities of research conducted on the mechanism of vibratory stress relief method (VSR), but the lack of a specific mechanism, explaining the process, was tangible. Therefore, in this article, the mechanism of VSR was explained using a new finite element model by focusing on the welded residual stresses, being widely used in industry. To be more specific, the effect of resonant vibration on residually stressed specimens was investigated numerically and experimentally. To model the welding simulation, a volumetric moving heat flux was defined using Goldak's model in Abaqus/CAE. In addition, experiments were planned in a way to investigate not only the effects of vibration time, but also the effect of amplitude of the vibration. Residual stresses were measured using Incremental Centre Hole Drilling (ICHD) method. Finally, a mechanical shaker was designed and assembled to induce higher frequencies and larger amplitudes.

1. Introduction

Residual stresses are mechanical stresses that have been a matter of great interest in recent decades. In this vein, great deals of research have been conducted on the different scopes including residual stresses measurement [1, 2]; their effects on different solid materials like metals, composites and tissues, to name a few [3]; and the methods to change their amount in a desired trend [4]. Residual stresses could appear during manufacturing processes such as welding, machining, and additive manufacturing [5, 6]. Also, they could be introduced to parts of many machines and industrial components during the operation [7]. These mechanical stresses change the behavior of parts, especially when external loads are applied, and these changes usually have disastrous effects on dimensional stability and fatigue life of loaded parts [8, 9]. Thus, it is important to investigate residual stresses and know how they affect the behavior of structures [10]. In this vein, it is necessary to study how to remove or reduce them in structures; residual stress relief has been investigated for several decades [11, 12]. The usual and traditional method is TSR (Thermal Stress Relief), having many disadvantages such as cost deficiency as well as time and energy consumption. Regarding these restrictions, a method has been provided in which residual stresses are removed using mechanical vibration. This method has several advantages over the TRS such as independence from temperature, preservation of energy and time, and reduction of costs.

* Corresponding author
E-mail address: a.h.mahmoudi@basu.ac.ir, a.h.mahmoudi@gmail.com (A.H. Mahmoudi)
https://doi.org/10.22099/ijmf.2020.38036.1164

VSR is practicable at room temperature by applying external loads on a residually stressed region so that the local plasticity takes place at that region [13, 14]. The most important prerequisite in loading is that the algebraic summation of residual and applied stresses must exceed the yield stress of the material [15]. If local plasticity happens, the residual stresses would be released up to the extent that the summation of residual and applied stresses on each point would exceed the yield stress of the specimens. The larger the summation of these stresses, the more relieved residual stresses will be. Considering these key points is crucial to help obtain better results:

- If the final goal is dimensional stability, it is not necessary to relieve all residual stresses [16, 17].
- Resonant frequencies in different mode shapes must be determined. The higher the frequency, the better the result [18].

Since real-world structures are large and contain complicated residual stress distribution, it is hard to apply large loads so that the superimposing of residual and applied stresses would be larger than the yield stress. Additionally, if the resonance phenomenon occurs, large strain and displacement can be obtained, not necessitating the presence of large forces to be applied. Based on Hooke's law, these large amounts of strains lead to large amounts of stresses [19]. This explanation manifests why and how VSR happens by applying vibration in the room temperature. A brief literate of the VSR is provided in the next paragraph.

McGoldrick and Saunders [20] conducted the first VSR experiment on welded and cast frames, without being aware of its mechanism. Lokshin [21] performed VSR on cast aluminum rings and succeeded in relieving 70 percent of residual stresses. Klauba and Adams [22] showed that the reduction of residual stresses is due to the occurrence of local plasticity phenomenon in the structure. Claxton [17] drew a comparison between vibratory and thermal stress relieving methods and suggested that VSR was not a proper substitution for PWHT (Post Weld Heat Treatment). Munsi et. al [23] evaluated VSR based on fatigue life of specimens. Hahn [24] provided a finite element model about VSR in his paper for the first time. Rao et. al [25] suggested an analytical equation to predict the amount of relieved residual stresses, focusing on cyclic creep and the theory of plasticity. Xu et. al [26] studied the effect of vibratory weld conditioning on the residual stresses and distortion in girth-butt welded pipes, having been developed based on VSR. Walker [18] noticed that the reason for relieving partial residual stresses is the initiation of the transformation of retained austenite particles by the movement of dislocations into positions that are favorable for the nucleation of martensite embryos. He et. al [27] studied the high-frequency VSR on some quenched specimens. Lv [28] suggested a novel method based on combining thermal and vibratory methods. Gao et. al [29] focused on fatigue life of an aluminium alloy treated by vibratory stress relief. Ebrahimi et. al [30] conducted a research to investigate the effects of frequency and amplitude of loading on VSR. Chen et. al [31] compared three stress relief methods (Thermal stress relief (TSR), vibratory stress relief (VSR), and thermal-vibratory Stress relief (TVSR)) in their investigation on an aluminium alloy.

Based on the literature history, a diverse array of research has been conducted on the mechanism of vibratory stress relief method, but a specific mechanism to explain it has not been proposed yet. Therefore, in this paper, the mechanism of VSR was explained using a new finite element model. Specifically, the effect of time and amplitude of resonant vibration on residually stressed specimens was numerically and experimentally studied. Finally, since welding is one of the most important topics in the industry, upon which residual stresses have major effects, VSR was investigated on some welded specimens.

2. Material and Methods

Regarding the diverse range of applications of stainless steels in the industry, austenite stainless steel was selected as material. The specimens had to have dimensions so that the natural frequency of the system would be lower than the maximum applicable frequency of the vibrator. Therefore, the proper dimensions of the specimens were obtained by modifying the specimen's

dimensions via simulations. Hence, the experimental approach became available because the natural frequency of the system would be lower than the maximum applicable frequency of the vibrator.

According to the tensile test, the stress-strain diagram was introduced to Abaqus. The mechanical and other properties of austenite stainless steel were defined for the Abaqus as new material. These properties included elastic and plastic properties, density, and Poisson's ratio as well as heat expansion coefficient, thermal conductivity, and specific heat. All these properties are presented in Table 1 through a wide range of temperatures (15-1500 °C).

As shown in Fig. 1, the specimen was connected to a Zwick instrument, located at Bu-Ali Sina University (Adobe Photoshop CS6 was used for removing background). Due to the restriction of loads, amplitudes, and frequency of vibrations, another instrument was designed. The designed instrument should have been able to produce reciprocating harmonic displacements to stimulate the plates in their natural frequency [32]. Having determined its location, the instrument was bolted to ground according to Fig. 2.

Table 1. Imported material properties of the specimen to Abaqus [33]

Temperature	conductivity (W/m°C)	Poisson's Ratio	Density (kg/m^3)	Specific Heat (J/kg°C)	Yield Stress (MPa)	Heat Expansion Coefficient (1/°C)
20	15	0.278	8030	492	350	1.53E-05
200	17.5	0.288	8010	502	270	0.000017
400	20	0.298	7960	514	193	1.81E-05
600	22.5	0.313	7920	526	153	1.88E-05
800	25.5	0.327	7880	538	112	1.94E-05
1000	30	0.342	7790	550	72	1.94E-05
1200	40	0.35	7690	562	14.5	1.94E-05
1340	55	0.351	7500	575	10	1.94E-05
1390	60	0.353	7450	587	5	1.94E-05
1500	62.2	0.49999	7450	599	0.000001	1.94E-05

Fig. 1. Experiment set-up for the vibration using the Zwick instrument.

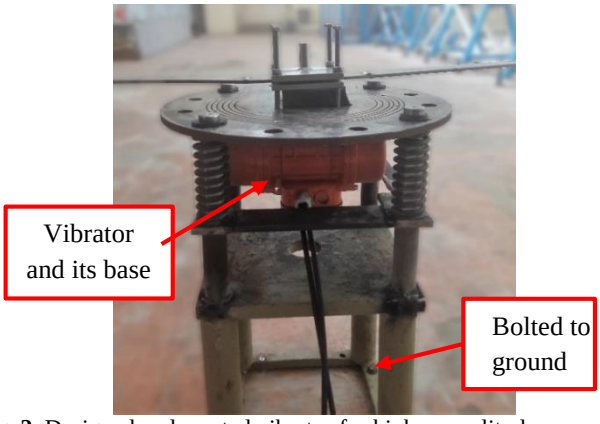

Fig. 2. Designed and erected vibrator for higher amplitudes and frequencies.

3. Finite Element Modeling

To simulate the VSR, a three-step analysis was performed: welding analysis (Sequentially coupled thermal-stress analysis), modal analysis, and dynamical loading. As the FE model was not a fully coupled thermal-stress analyzer, heat transfer could have been affected by the melting material during welding, giving rise to an error. However, this error was neglected because it was a bead-on-plate welding. In this type of welding, the welding pass is only one and does not affect the heat pool [34].

Element type, element family, and solver type were selected based on the model and simulations. ABAQUS/CAE 6-12.3 was used for all simulations. Second-order elements (DC3D20) were used in all analyses except for modal analysis. As it was not practical to use this element type for modal analysis, linear elements were used for the model (700000 linear elements). Furthermore, a Fortran subroutine code was linked to ABAQUS for defining Goldak's heat source model for bead-on-plate welding simulation [35]. In the finite element model, it was required to monitor the elements' stresses history during resonance in the loading step; therefore, the implicit dynamic solver was used.

According to Goldak's model, the heat model for welding is a moving three-dimensional heat flux in which two heat fluxes, for both the front and rear of the torch, are used. Equation 1 and equation 2 [35] represent the body heat fluxes, and all the parameters are defined in Table 2 and Table 3.

$$q_f(x,y,z) = \frac{6\sqrt{3}f_f\eta Q}{a_f bc\pi\sqrt{\pi}} \exp\left(-\frac{3x^2}{{a_f}^2} - \frac{3y^2}{b^2} - \frac{3z^2}{c^2}\right) \quad (1)$$

$$q_r(x,y,z) = \frac{6\sqrt{3}f_r\eta Q}{a_r bc\pi\sqrt{\pi}} \exp\left(-\frac{3x^2}{{a_r}^2} - \frac{3y^2}{b^2} - \frac{3z^2}{c^2}\right) \quad (2)$$

Table 2. Parameters for Goldak's model

Parameter	Description	Parameter	Description
x, y, z	Coordinate parameters	η	Efficiency of the arc
Q	From Equation 3 [36]	f_r, f_f	From Equation 4 [36]
a_r, a_f, b, c	From Fig. 3		

$$Q = VI \quad (3)$$

$$f_r = \frac{2a_f}{a_r+a_f}\ , f_f = \frac{2a_r}{a_r+a_f} \quad (4)$$

The electric arc welding (SMAW) was performed on a provided stainless-steel plate. To obtain steady residual stresses along the welding path, the plate was welded before being divided into small specimens as shown in Fig. 6. The initial width of the plate was 300 mm at first. As the width of each specimen was 40 mm, 7 specimens were created from that plate. Residual stresses at the beginning and the end point of the welding procedure, especially at the beginning, are different from those at mid-points of the welded path [37]. To neutralize this effect, two metal pieces were placed on the beginning and the end points of the welding path so that the start point and the end point of the welding happened on these metal pieces. The residual stresses get changed by distancing from the welding line. However, if there is one pass of the weld bead, except the beginning and end of that bead, the contour of residual stresses will be the same for each section perpendicular to the weld bead. As the endpoint and start point of welding were out of the area that specimens were cut, it was a safe assumption that specimens had the same contours of residual stresses along with the weld bead. The relevant geometrical parameters of welding recorded [38]. Also, the parameters, being used to define the heat input in simulations, are presented in Table 3.

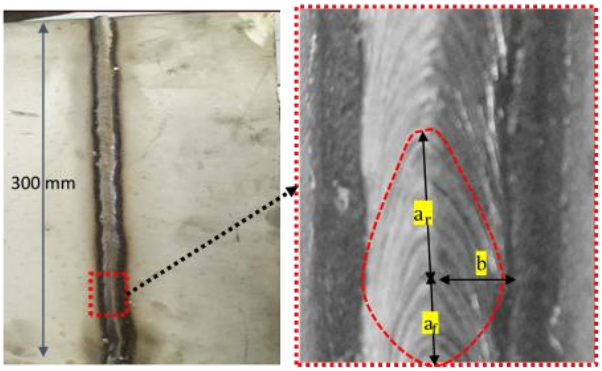

Fig. 3. The welded plate and geometric parameter for modelling the welding simulation.

Table 3. welding parameters for simulation of welding process

Voltage	30 v
Current	100 A
Ambient Temperature	3°C (winter in Hamedan)
Cooling Duration	30 minutes
Torch Speed	4.67 mm/s

4. Results and Discussion

In this part, the numerical and experimental results are illustrated in the form of different figures. First, the results of the simulations are presented and discussed. Then, the experimental measurements are reported in different figures and compared with each other. Finally, a comparison is drawn between numerical and experimental results to verify the numerical results.

4.1. Results of simulation

The welding simulation and the simulation of different loading mechanisms are illustrated in the following section. Element size was studied as such, it was concluded that the 1 mm for the element size was optimum.

4.1.1. Results of welding simulation

According to a drawn comparison between the Fusion Zone (FZ) of the experimental and numerical models, which are shown in Fig. 4, the welding simulation predicted reliable results. The gray section in this contour experienced temperatures above 1530 °C. The same work was performed for the Heat Affected Zone (HAZ) and a geometrical comparison is shown in Fig. 5.

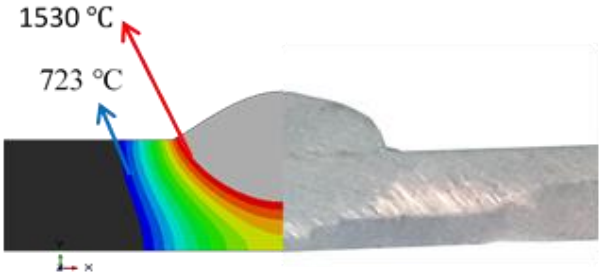

Fig. 4. Geometrical comparison of Fusion Zone between specimens and the FE model.

Fig. 5. Geometrical comparison of Heat Affected Zone between specimens and the FE model.

4.1.2. Results of loading

In this part, two cases of simulations have been studied and presented. Firstly, the results and figures of three different amounts of loading were presented and discussed. Then, the history of residual stresses on an element, which was under the strain gage in the real-world situation, was provided in order to open up a new window of understanding how VSR works.

4.1.3. Different loadings

Several states of loading in resonance condition according to experiments were simulated. In these simulations, the supports were harmonically excited at the natural frequency of the system by amplitudes of ±25 mm, ±50 mm, and ±75 mm. In this paper, the vibration of support with amplitude "a" has represented as "±a" for abbreviation. Furthermore, the words longitudinal and transverse stresses have been used to show these parameters with respect to the weld line. In all diagrams, the amount of displacements of supports, the input of the vibratory system, was shown by "fixed end displacement" (FiED). Also, displacement of the free end of the plate, the output of the system, was shown by "free end displacement" (FrED).

Residual stresses were illustrated in two longitudinal and transverse paths to evaluate the effects of time and amplitude of the loadings. The paths for depicting residual stresses and dimensions of specimens were shown in Fig. 6. These dimensions were the result of the simulation, adapting the specimens' size to an applicable frequency with the current instrument. In addition, the locations of strain gages, being the nearest attachable points to the weld bead on the top and bottom of plates, were shown in Fig. 6.

Residual stresses before and after vibrations for transverse stresses are illustrated in Fig. 7. According to these curves, the amount of relieved residual stresses increased as a result of an increase in the inputted amplitude. In other words, the more the amplitude of excitation, the more the relief of residual stresses. Based on this figure, the transverse residual stresses reduced up to 50 MPa for the best state. Similar results were obtained for longitudinal residual stresses.

The longitudinal stresses are shown in Fig. 8. Based on the theory discussed in the introduction, it was expected that for 0.50 mm FiED the level of residual stresses after vibration comes exactly between the diagrams of 0.25 mm FiED and 0.75 mm FiED. However, in these curves, it is obvious that for both loading 0.50 mm and 0.75 mm high amounts of residual stresses have been relieved, ending with the same amount of residual stresses after the vibration in both cases. In fact, the reason is that 0.50 mm FiED relieved almost all longitudinal residual stresses. Therefore, when 0.75 mm FiED applies, there were not any considerable amounts of residual stresses left to be relieved. Hence, both 0.50 mm and 0.75 mm loadings could lead the experiments to their optimum results in terms of the longitudinal stresses.

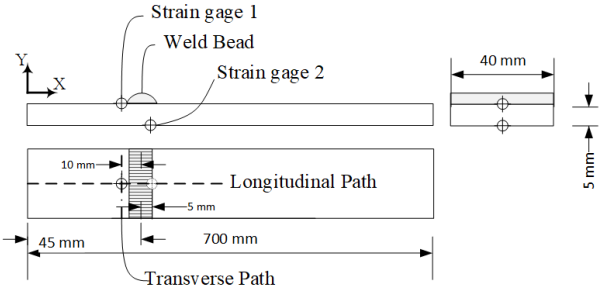

Fig. 6. Paths for depicting residual stresses and dimensions of specimens.

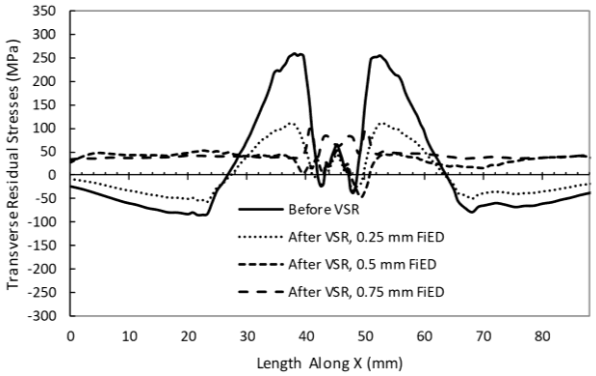

Fig. 7. Transverse stresses along a portion of transverse path.

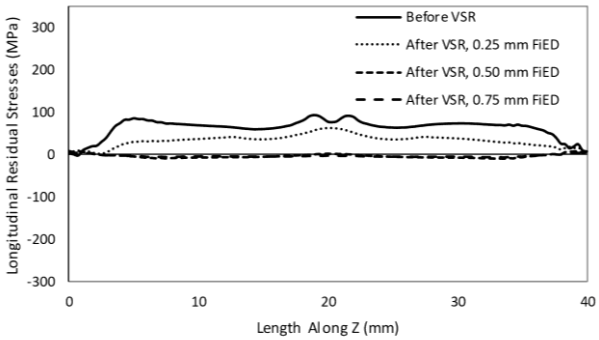

Fig. 8. Longitudinal stresses along the longitudinal path.

4.1.4. Element history

In the first part of this section, the mechanism of VSR is discussed; then, stress history diagrams have been illustrated for different loadings. The history of residual stresses on an element, being under the real strain gage in specimens, is provided in this section. The position of these elements on the model, with respect to the welding bead, is shown in Fig. 9. Initially, the plate was vibrated for 120 seconds; equivalent to the initial 1000 cycles at the resonance frequency (based on modal analysis simulation, the first natural frequency in the bending mode-shape of the system was 8.33 Hz). According to Fig. 10, the amount of average stress was reduced during the initial seconds. In Fig. 11, being the magnified figure of Fig. 10, the curve became approximately stable after almost 4.5 seconds. Hence, in order to reduce the computational costs, the rest of the simulations were performed for 5 seconds.

It was essential to specify a criterion to study the residual stresses in these curves. As the applied force was harmonic, it was expected that the response of the system to this load would have been harmonic as well

(based on the theory of vibration). Hence, the free end of the plate followed a harmonical movement. This meant that the applied stresses to every point in the plate, including the monitored element, would have followed a harmonical trend over time. Therefore, the deduced stresses were expected to be harmonic as well. Consequently, using the principle of superimposing forces, the oscillation around average stresses in Fig. 11 are the result of harmonic loads. Also, the average line of stress history is representative of the residual stresses of the considered elements. Since the purpose of this paper was studying residual stresses, the average line was a good criterion for such studies.

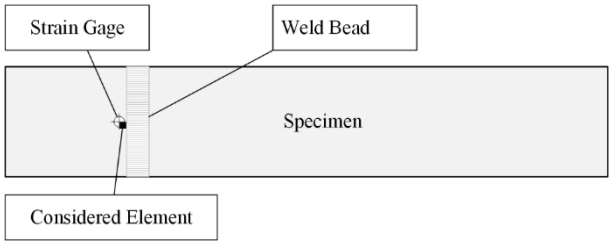

Fig. 9. Position of the chosen elements on the model.

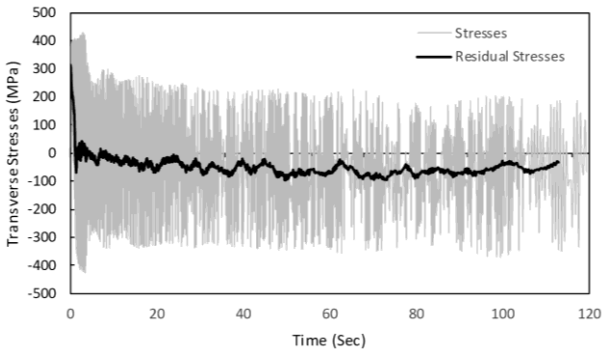

Fig. 10. Transverse residual stresses on the considered element for 120 seconds.

As mentioned in the introduction, the basic rule of performing a successful VSR is that the algebraic summation of loading and residual stresses must exceed the yield stress of the material. The upper and lower bounds of the diagram, being depicted in shaded lines, were the algebraic summation of loading and residual stresses in the considered element at any specific time. It was obvious that the upper bound of the diagram was restricted by the horizontal line, referring to the yield point of the material. Based on the theory, it was expected that by reaching to yield stress the stress relief starts; this meant a decline in the residual stress amount, the average line in Fig. 11. The more this situation continued, the more residual stresses got relieved. This trend continued until there was not any surpassing from the yield stress. From this moment out, the residual stresses did not change anymore because there were either no existing residual stresses at that point or the summation of the applied stress and the residual stress could not surpass the yield stress.

A closer look at the initial steps in Fig. 11 showed that when the shaded diagram has crossed the horizontal line, residual stresses have started to decline. After that, the more time passed, the more the residual stresses reduced. As it was shown, after 1.5 seconds, the residual stresses' curve reached zero, and after 4.5 seconds, the curve became virtually stable.

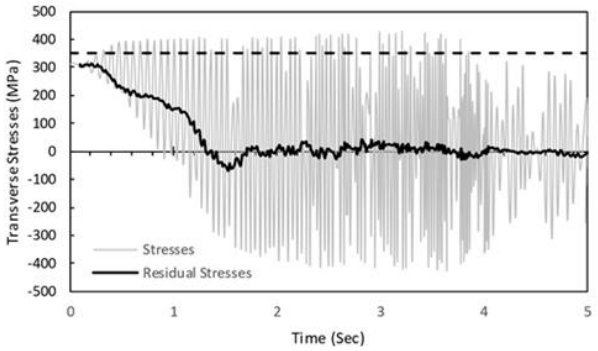

Fig. 11. Transverse residual stresses on the considered element during 0 to 5 seconds.

The stress relieving initiated before stabilization of the vibrational system. To be more specific, the residual stresses in the specimen after welding were near the yield stress. Consequently, although the loading stresses were small at the beginning of vibration, the algebraic summation of loading and residual stresses could be bigger than the yield stress. Therefore, the amount of residual stresses was reduced in a way that the algebraic summation of residual and loading stresses was equal to the yield point. In fact, the amounts of residual stresses that have made the summation exceed the yield point have been relieved. Thus, the cycle-to-cycle reduction of the residual stresses was supported by cycle-to-cycle

increasing of applied stresses due to resonance. Besides that, the resonance phenomenon has begun, and consequently, the amplitude of the applied stresses has increased. Hence, the residual stresses dramatically plunged to the extent that almost all of them were relieved.

Furthermore, it was expected that after vibrations get stable, the upper bound of the shaded curve stay on 400 MPa. However, according to Fig. 11, after stress relief, this amount became less than yield point and remained stable there. The reason for this phenomenon was the subtle reduction of natural frequency, being affected by the reduction of residual stresses. In fact, increasing residual stresses hardened the specimens, and by hardening, the natural frequency of specimens increased.

The history of transverse stresses at the first 5 seconds of vibration for elements below the hole of the strain gage for FiED 0.25 mm, 0.50 mm, and 0.75 mm are shown in Fig. 12. According to these diagrams, representing the history of transverse residual stresses on the considered element for several amounts of FiEDs, the bigger the amplitude of vibration, the faster the residual stresses relief. Residual stresses were reduced to almost zero for all FiEDs while no such results were observed in diagrams of the residual stresses paths (Fig. 7 and Fig. 8). The reason was that the amount of reported stress in Fig. 12 has been calculated from 27 integration points of the considered 20 nodes on its borders (these elements were 3D and of second-order) [39]. Conversely, the amount of reported residual stresses along the paths has been the exact amount of the nodal stress.

Moreover, the history of longitudinal stress curves for several states of vibrations are represented in Fig. 13. Despite the variation of transverse stresses, longitudinal components of stress tensor had no high oscillations. This was because of the fact that resonance happened so that it excited the plate in the bending mode. As bending of the plate imposed larger transverse stresses than longitudinal stresses (see Fig. 6), applied stresses of this mechanism, which were supposed to be added to the residual stresses, caused slower stress relieving for the longitudinal residual stresses rather than the transverse residual stresses. In addition, the amounts of transverse residual stresses were reduced much quicker than that of longitudinal stresses. This can be attributed to the mechanism of loading: since the excited mode was bending around axis Z, the deduced normal stresses were along axis X, so according to relations between bending forces on a plate and normal stresses, Equation 5 [19], the major loading stresses were in the X direction.

$$\sigma_x = My/I \quad (5)$$

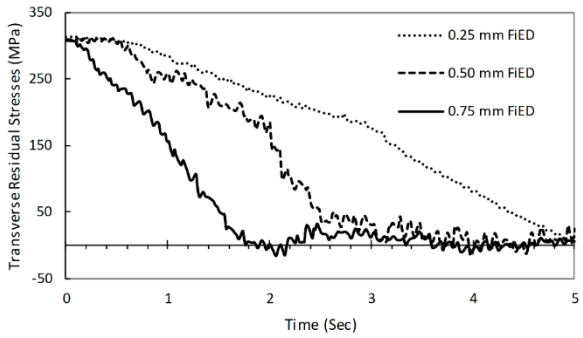

Fig. 12. History of transverse stresses.

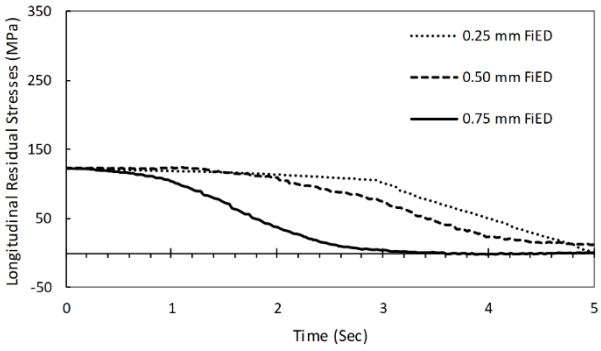

Fig. 13. History of longitudinal stresses.

Another noticeable point was that the initial longitudinal stresses were less than the initial transverse stresses. For this reason, the required time for transverse residual stresses to get relieved was less than the required time for longitudinal residual stresses. (in Fig. 12 for 0.75 mm FiED, the stable state was achieved in 1.7 Sec, but in Fig. 13 in 2.7 Sec.). The reason was that the induced stress by vibrations was not large enough at first, but as the FrED increased, the summation of residual and vibratory stresses reached the level of yield stress, leading to residual stress relieving.

4.2. Experimental results

The measurement of residual stresses of the specimens were performed at the laboratory of residual stresses and mechanical behavior of materials, located in the Bu-Ali Sina University of Hamedan, Iran [40]. In total, 12 measurements were implemented using the method of Incremental Center-Hole Drilling (ICHD). This technique works by measuring strains when part of the component was machined away. Then, the specimen relieves the equivalent residual stresses that were presented in the removed section before drilling. In fact, this method measures the equivalent strains due to the existence of residual stresses. The beauty of the incremental method is that it can measure the residual stresses almost near the yield stress of the specimen which was impossible in the previous methods. Six test samples were prepared and the tests were planned in a way to investigate the effects of vibration time as well as the variation of FiED. Moreover, a pair of measurements were done for the specimen that had vibrated with the designed vibrator.

4.2.1. Study of fixed end displacement effect

In this section, three states of applied vibrations were studied. An unloaded specimen, which was supposed to determine initial residual stresses, was considered as the reference specimen. Six measurements were performed on the location of the first strain gage (see Fig. 6). To be more specific, four measurements were performed to study the effect of base displacement on each strain gage point (one before and three after vibrations). The results of longitudinal stresses are shown in Fig. 14. In these curves, the horizontal axis represents the depth of drilled holes. As it was expected, by increasing the amplitude of excitation, the amounts of relieved residual stresses increased.

The transverse stresses are depicted in Fig. 15 for different FiEDs. In this figure, the amount of relieved stresses was equivalent to excitation amplitude. Since FrED increased by approaching resonance, bigger bending stresses applied to the specimen, especially at its base. Furthermore, the transverse stresses in the second point of measurement are depicted in Fig. 16. In this diagram, the transverse residual stresses were reduced from 350 MPa to somewhere between 100 MPa and 140 MPa.

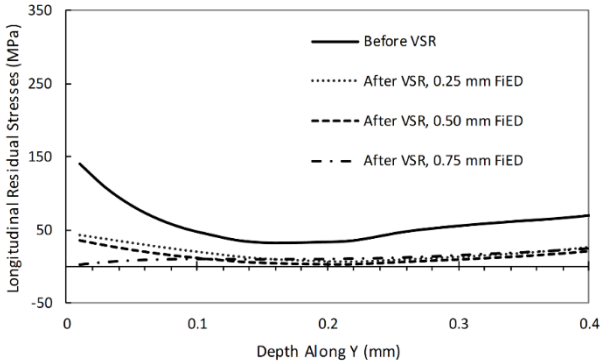

Fig. 14. Longitudinal stresses for different FiEDs (first point of measurement).

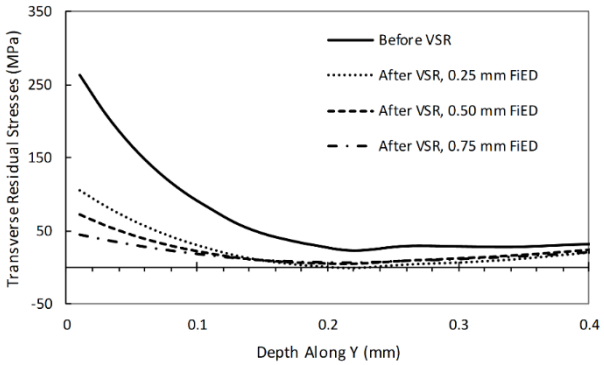

Fig. 15. Transverse stresses for different FiEDs (first point of measurement).

According to Fig. 17, the longitudinal residual stresses were reduced in all cases. In the shown diagrams, based on the previous paragraph, for Fig. 14, Fig. 15, and Fig. 17, the best result was achieved when FiED was equal to 0.75 mm. Admittedly, according to transverse residual stress results, Fig. 16, the result of 0.50 mm FiED was the best. However, the results were very close to each other and this unexpected result could be neglected. Thus, by increasing the amplitude of the vibration, larger amounts of residual stresses were relieved.

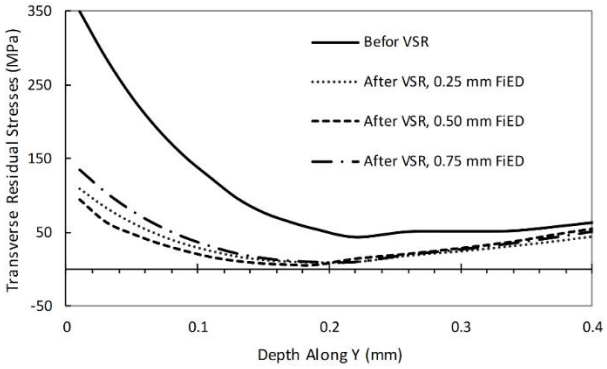

Fig. 16. Transverse stresses for different FiEDs (second point of measurement).

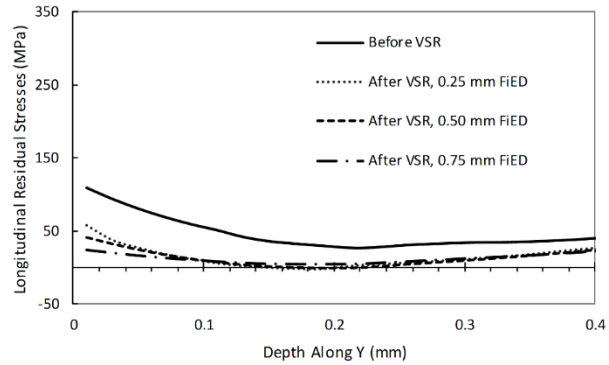

Fig. 17. Longitudinal stresses for different FiEDs (second point of measurement).

4.2.2. Effect of time of vibration

In this section, the effect of time on vibratory stress relief has been studied. Based on sec 4.1, the results of simulations showed that the time of vibration does not affect the amount of relieved residual stresses, and its diagram became stable after about 5 seconds; although this stability depended on some parameters. Observation in these trends led to an explanation for the mechanism of VSR.

Additional to the theory of plasticity, two other theories were used to explain the mechanism of vibratory stress relief. Firstly, the history of the average dynamic creep conducted by Rao et. al [25], and secondly, the transformation model of retained austenitic particles suggested by Walker [18]. In the latter model, the relieving of residual stresses was attributed to the transformation of retained austenite particles to some positions for the nucleation of martensite embryos. The amount of relieved residual stresses' level in Walker's theory is not too large, so the changes in residual stresses that were made after initial cycles could be explained using this theory. Thus, a combination of both these models could explain the behavior of the material: Based on the theory of plasticity, major variation in residual stresses happens in the initial cycles. The theory of plasticity has no clarifying explanation regarding stress relieving after the initial cycles. In this case, the behavior of the material can be explained according to the theory of transformation of retained austenite particles. Accordingly, the reason for partially relieving residual stresses was related to the beginning of transformation of the retained austenite particles to some positions for the nucleation of martensitic embryos.

In the first measurement point, according to Fig. 18, the time of vibrations had no remarkable effect on the longitudinal vibrations. Moreover, based on Fig. 19, the effect of time on transverse stresses was low, which can be explained by Walker's theory.

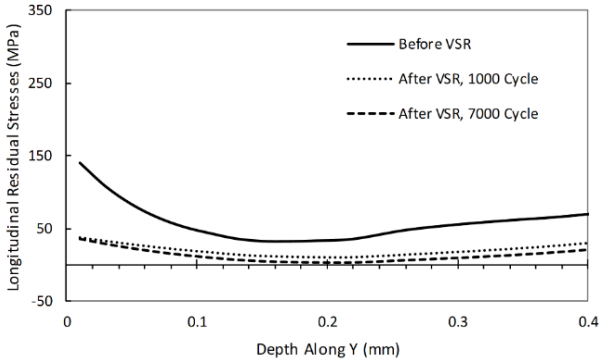

Fig. 18. Effect of time of vibration on longitudinal residual stresses for the first point of measurement.

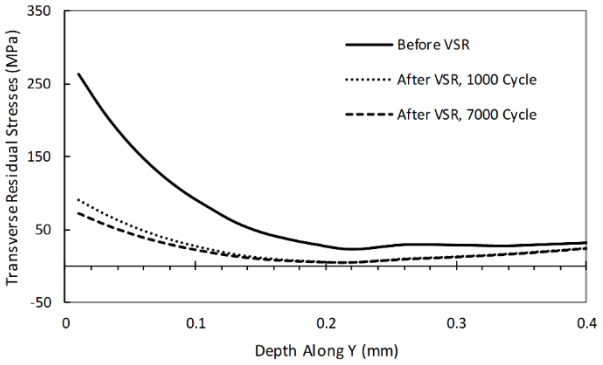

Fig. 19. Effect of time of vibration on transverse residual stresses for the first point of measurement.

For the second measuring point, by letting specimens vibrate for a longer time, larger amounts of transverse stresses got relieved. For different vibrating times for transverse stresses (Fig. 20), it was observed that the time of vibration was effective on stress relief at this point. In fact, the only difference between measurement points was their stiffness: The stiffness of point 2 was increased due to its high-temperature history because of its adjacency to the welding torch (see Fig. 6). Accordingly, the stiffness of the sample in the second measurement point has increased, and relieving of residual stresses was further delayed. To be more specific, in the next 6000 cycles, the transverse residual stresses changed from 200 MPa to 100 MPa (The level of residual stresses had been 350 MPa). As a result, VSR will be more successful for more ductile metals, and for stiffer metals more time is needed to have successful stress relief. Moreover, the longitudinal stresses at different vibration times are shown in Fig. 21. Likewise, the stress relief was dependent on time, and during the initial cycles, the residual stresses were necessarily not relieved.

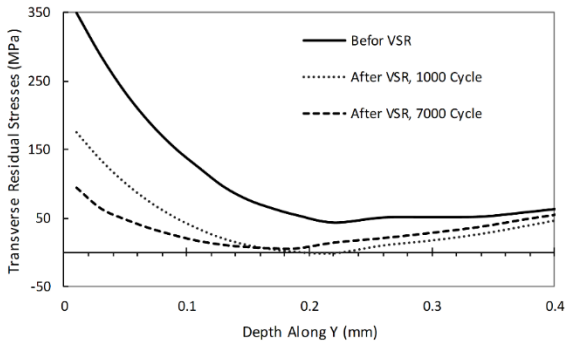

Fig. 20. Effect of time of vibration on Transverse residual stresses for the second point of measurement.

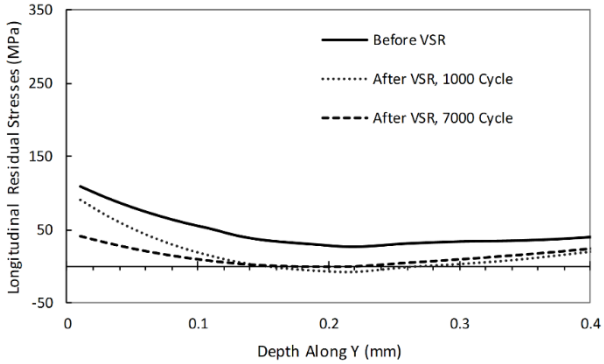

Fig. 21. Effect of time of vibration on longitudinal residual stresses for the second point of measurement.

4.2.3 The vibrated sample by constructed vibrator

Vibratory stress relief was done using a vibrator instrument, designed and constructed during this research. In Fig. 22 and Fig. 23 the diagrams of transverse and longitudinal residual stresses are illustrated, respectively. The results obtained for both transverse and longitudinal stresses were remarkable in the performed tests by the constructed instrument. Admittedly, the results of the Zwick instrument were better than the results of the constructed instrument. In fact, the chosen result of the Zwick instrument was considered to be the best one, which was 0.75 mm FiED. However, for such a cost-effective device, achieving to, approximately, the same result as Zwick was quite impressive.

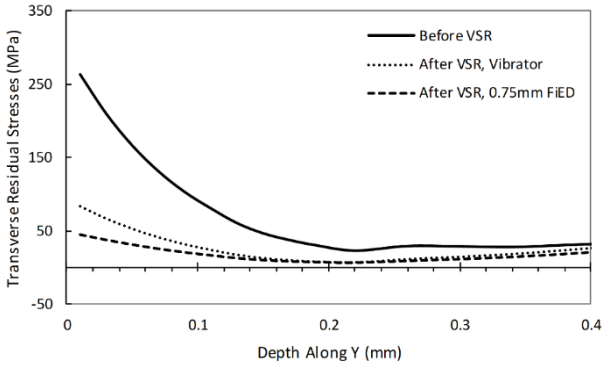

Fig. 22. Vibratory stress relieving of transverse stresses using constructed vibrator.

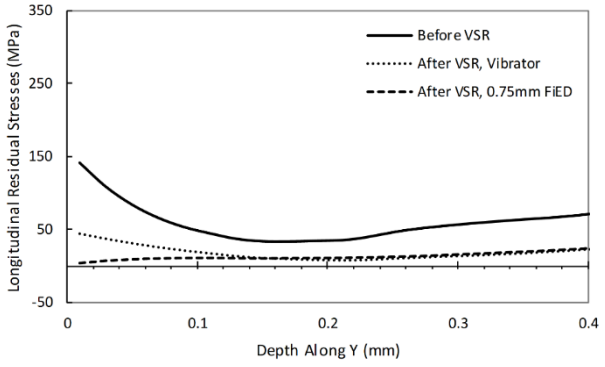

Fig. 23. Vibratory stress relieving of longitudinal stresses using constructed vibrator.

4.3. Comparison of results

In this part, the results of simulations have been validated by the experimental results. The path of depicting stress in the numerical model is represented in Fig. 24. The experimental results in a drilling path were

compared with the numerical results of the same path. For both transverse and longitudinal stresses, numerical and experimental results showed a good agreement.

In Fig. 25 and Fig. 26, the experimental and numerical results of residual stresses for transverse and longitudinal stresses were, respectively, compared. Since the comparison was performed before welding, it could be considered as a validation for welding simulation, as well.

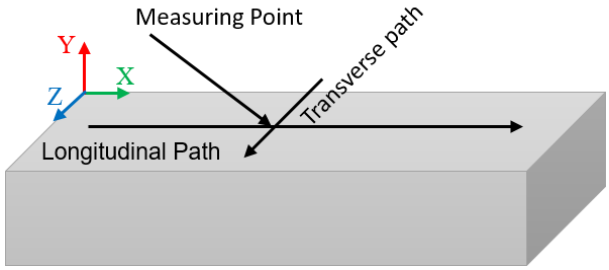

Fig. 24. paths of stresses in FEM and drilling.

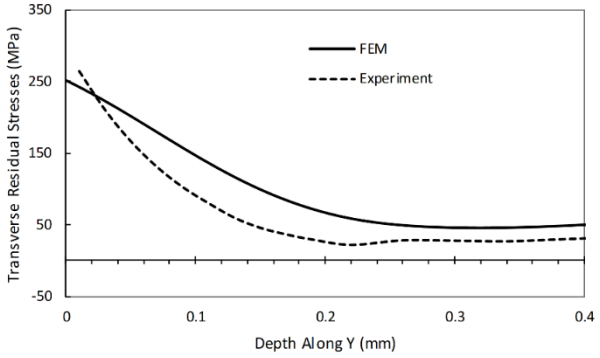

Fig. 25. Numerical and experimental comparison of transverse residual stresses before vibration.

The comparison of numerical and experimental results for transverse stresses in the first point of measurement is given in Table 4. The same comparison for longitudinal stress is shown in Table 5. The reduction percent in these tables showed the percentage of relieved residual stresses in comparison with their initial amounts in both the numerical and experimental results. In fact, the percentage of reduced amounts was considered as the comparative result in experiments and simulations. The maximum error was from longitudinal stresses for 0.25 mm FiED. However, except that one, the other results were relevant, and showed the efficiency of the numerical method for simulation. Therefore, the performed analyses, using this numerical method, were valid and reasonable.

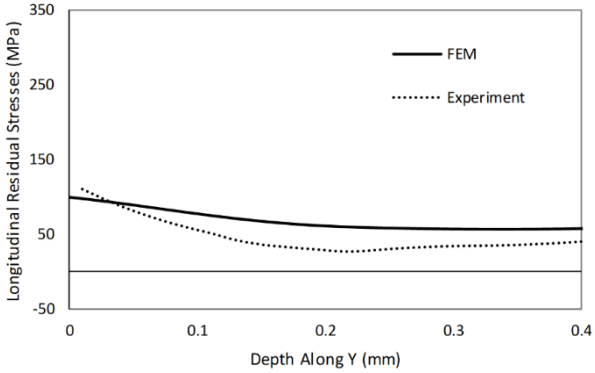

Fig. 26. Numerical and experimental comparison of longitudinal residual stresses before vibration.

Regardless of the comparison of the numerical and experimental results, the stress relief in real specimens was remarkable. The minimum and maximum amounts of relieving residual stresses were 59.99% and 97.57%, respectively, and this was an acceptable and satisfying result.

Table 4. Numerical and experimental results for transverse residual stresses in the first point of measurement

	Numerical Results			**Experimental Results**			
	Residual Stresses (MPa)	Relieved Stresses (MPa)	% Reduction	Residual Stresses (MPa)	Relieved Stresses (MPa)	% Reduction	Error
Before Vibration	257	-	-	263.74	-	-	-
FiED 0.25 mm	109	148	57.59	105.51	158.23	59.99	2.4
FiED 0.50 mm	41.3	215.7	83.93	72.402	189.338	71.79	12.14
FiED 0.75 mm	37.0	220	85.6	45.69	218.05	82.67	2.93

Table 5. Numerical and experimental results for longitudinal residual stresses in the first point of measurement

	Numerical Results			Experimental Results			
	Residual Stresses (MPa)	Relieved Stresses (MPa)	%Reduction	Residual Stresses (MPa)	Relieved Stresses (MPa)	%Reduction	Error
Before Vibration	113	-	-	141.05	-	-	-
FiED 0.25 mm	74.2	38.8	34.33	42.733	98.317	69.70	35.37
FiED 0.50 mm	19.1	93.9	83.10	35.299	105.571	74.85	8.35
FiED 0.75 mm	6.39	106.61	94.34	3.4212	137.6288	97.57	3.23

5. Conclusions

Vibratory stress relief was performed to study the effect of amplitude and time of vibration. After measuring residual stresses using the Incremental Center-Hole Drilling (ICHD) method, investigations showed that the amplitude of excitation, on both longitudinal and transverse stresses, was more effective than the time of vibration. Finally, the general results achieved from the simulations and experiments have been presented below.

1- As was expected, the more the amplitude of excitation, the more the amount of relieved residual stresses was.

2- By using residual stresses histories on elements and also the experimental results, it was shown that VSR happens in the first cycles.

3- The stiffer the material, the later the VSR will take place.

4- Generally, the residual stresses were reduced uniformly and the time of vibration had no remarkable effect on this matter. However, in some cases, the relieved residual stresses were bigger for cases with more time under vibration. These results were explained using the model of retained austenite particles.

5- The results achieved from the constructed instrument were noteworthy. However, in a comparison, these results were not better than the results of the Zwick instrument.

6- The simulations for different cases of loading in resonance conditions were completed using a dynamic implicit model. In these simulations, the support was vibrated by amplitudes of 0.25 mm, 0.50 mm, and 0.75 mm at the natural frequency of the system.

7- Regardless of the comparison of the numerical and experimental results, the stress relief in specimens was notable. The minimum and maximum amounts of relieved residual stresses were 59.99% and 97.57%, respectively, and this was an acceptable and satisfying result.

8- According to the fact that the amount of removed residual stresses after initial cycles was low but not negligible, in some cases, the theories of transfer of the retained austenite particles and plasticity were combined to introduce a new model to explain the mechanism of the VSR.

6. References

[1] G. S. Schajer, Practical residual stress measurement methods, John Wiley & Sons, 2013.

[2] A. Mahmoudi, D. Yoosef-Zadeh, and F. Hosseinzadeh, Residual Stresses Measurement in Hollow Samples Using Contour Method, *International Journal of Engineering*, 33(5) (2020) 885-893.

[3] K. Zhu, Z. Li, G. Fan, R. Xu, and C. Jiang, Thermal relaxation of residual stress in shot-peened CNT/Al–Mg–Si alloy composites, *Journal of Materials Research and Technology*, 8(2) (2019) 2201-2208.

[4] X. Liu, J. Liu, Z. Zuo, and H. Zhang, Numerical study on residual stress redistribution of shot-peened aluminum 7075-T6 under fretting loading, *International Journal of Mechanical Sciences*, 160 (2019) 156-164.

[5] K. Hemmesi, P. Mallet, and M. Farajian, Numerical evaluation of surface welding residual stress behavior under multiaxial mechanical loading and experimental validations, *International Journal of Mechanical Sciences*, 168 (2020) 105-127.

[6] X. Song, S. Feih, W. Zhai, C.N. Sun, F. Li, R. Maiti, J. Wei, Y. Yang, V. Oancea, L.R. Brandt, A.M. Korsunsky, Advances in additive manufacturing process simulation: Residual stresses and distortion predictions in complex metallic components, *Materials & Design*, (2020) 108779.

[7] D. Ulutan, B. E. Alaca, and I. Lazoglu, Analytical modelling of residual stresses in machining, *Journal of Materials Processing Technology*, 183(1) (2007) 77-87.

[8] M.N. James, D.J. Hughes, Z. Chen, H. Lombard, D.G. Hattingh, D. Asquith, J.R. Yates, and P.J. Webster, Residual stresses and fatigue performance, *Engineering Failure Analysis*, 14(2) (2007) 384-395.

[9] C. Sonsino, Effect of residual stresses on the fatigue behaviour of welded joints depending on loading conditions and weld geometry, *International Journal of Fatigue*, 31 no. 1 (2009) 88-101.

[10] K. Masubuchi, *Analysis of welded structures: residual stresses, distortion, and their consequences*. Elsevier, 2013.

[11] Q. Zhang, L. Yu, X. Shang, and S. Zhao, Residual stress relief of welded aluminum alloy plate using ultrasonic vibration, *Ultrasonics*, (2020) 106-164.

[12] K. Chin, S. Idapalapati, and D. Ardi, Thermal stress relaxation in shot peened and laser peened nickel-based superalloy, *Journal of Materials Science & Technology*, (2020).

[13] I. K. Lokshin, Vibration treatment and dimensional stabilization of castings, *RUSS CAST PROD*, 10 (1965) 454-457.

[14] B. Klauba and C. M. Adams, Progress report on the use and understanding of vibratory stress relief, in *Proc. ASME Conf. on Productive Applications of Mechanical Vibrations, Phoenix, Arizona*, (1982) 47-58.

[15] S. Kwofie, Plasticity model for simulation, description and evaluation of vibratory stress relief, *Materials Science and Engineering: A*, 516(1-2) (2009) 154-161.

[16] G. Adoyan, The vibratory stress relieving of castings, *Machines and Tooling*, 38(8) (1967) 18-22.

[17] R. Claxton, Vibratory stress relieving- an effective alternative to thermal treatment for component stabilisation, *I. research, equipment and processing heat treatment of metals*, 18(2) (1991) 53-59.

[18] C. Walker, A theoretical review of the operation of vibratory stress relief with particular reference to the stabilization of large-scale fabrications, *Proceedings of the Institution of Mechanical Engineers, Part L: Journal of Materials: Design and Applications*, 225(3) (2011) 195-204.

[19] F. Beer, E. Johnston, and J. DeWolf, *Mechanics of materials, 2002* (McGraw-Hill, New York). 2002.

[20] R. McGoldrick and H. E. Saunders, Some experiments in stress-relieving castings and welded structures by vibration, *Journal of the american society for naval engineers*, 55(4) (1943) 589-609.

[21] I. K. Lokshin, Vibration treatment and dimensional stabilization of castings, *Russ cast prod*,10 (1965).

[22] B. Klauba and C. M. Adams, Progress report on the use and understanding of vibratory stress relief, *Proc. ASME Conf. on Productive Applications of Mechanical Vibrations, Phoenix, Arizona*, 47-58.

[23] A. Munsi, A. Waddell, and C. Walker, The influence of vibratory treatment on the fatigue life of welds: A comparison with thermal stress relief, *Strain*, 37 (4) (2001) 141-149.

[24] W. F. Hahn, Vibratory residual stress relief and modifications in metals to conserve resources and prevent pollution, in "Final Report, Alfred University, Center of Environmental and Energy Research (CEER)," 2002, [Online]. Available: https://cfpub.epa.gov/ncer_abstracts/index.cfm/fuseaction/display.abstractDetail/abstract/7803/report/F.

[25] D. Rao, D. Wang, L. Chen, and C. Ni, The effectiveness evaluation of 314L stainless steel vibratory stress relief by dynamic stress, *International Journal of Fatigue*, 29(1) (2007) 192-196.

[26] J. Xu, L. Chen, and C. Ni, Effect of vibratory weld conditioning on the residual stresses and distortion in multipass girth-butt welded pipes, *International Journal of Pressure vessels and piping*, 84(5) (2007) 298-303.

[27] W. He, B. P. Gu, J. Y. Zheng, and R. J. Shen, Research on high-frequency vibratory stress relief of small Cr12MoV quenched specimens, *Applied Mechanics and Materials*, (2012) 1157-1161.

[28] T. Lv and Y. Zhang, 1719. A combined method of thermal and vibratory stress relief, *Journal of Vibroengineering*, 17 (6) (2015).

[29] H. Gao, Y. Zhang, Q. Wu, J. Song, and K. Wen, Fatigue life of 7075-T651 aluminium alloy treated with vibratory stress relief, *International Journal of Fatigue*, 108 (2018) 62-67.

[30] S. M. Ebrahimi, M. Farahani, and D. Akbari, The influences of the cyclic force magnitude and frequency on the effectiveness of the vibratory stress relief process on a butt welded connection, *The International Journal of Advanced Manufacturing Technology*, 102(5) (2019) 2147-2158.

[31] S.G. Chen, Y.D. Zhang, Q. Wu, H.J. Gao, and D.-Y. Yan, Residual stress relief for 2219 aluminum alloy weldments: A comparative study on three stress relief methods, *Metals*, 9(4) (2019) 419.

[32] N. Anekar, V. Ruiwale, S. Nimbalkar, and P. Rao, Design and testing of unbalanced mass mechanical vibration exciter, *IJRET* (2014) 2321-7308.

[33] TotalMateria. (2017). *Totalmateria* [Online]. The world's most comprehensive materials database.

[34] G. Salerno, *C.* Bennett, W. Sun, A. Becker, N. Palumbo, J. Kelleher, S.Y. Zhang, On the interaction between welding residual stresses: a numerical and experimental investigation, *International Journal of Mechanical Sciences*, 144 (2018) 654-667.

[35] J. Goldak, A. Chakravarti, and M. Bibby, A new finite element model for welding heat sources, *Metallurgical transactions B*, 15(2) (1984) 299-305.

[36] C. A. Guang-Ming Fu, Marcelo Igor Lourenço, Meng-Lan Duan, Segen F. Estefen, Finite Element Modeling Of Transient Temperature And Residual Tress Distribution Analysis In Multi-Pass Welding Process, *ASME 2012 31st International Conference on Ocean* (2012).

[37] P. Bouchard, The NeT bead-on-plate benchmark for weld residual stress simulation, *International Journal of Pressure Vessels and Piping*, 86(1) (2009) 31-42.

[38] M. Zubairuddin, S. Albert, M. Vasudevan, V. Chaudhari, and V. Suri, Finite element simulation of weld bead geometry and temperature distribution during GTA welding of modified 9CR-1MO steel and experimental validation, *Journal for Manufacturing Science and Production*, 14(4) (2014) 195-207.

[39] ABAQUS, Abaqus Analysis User's Guide, vol. VOLUME IV: ELEMENTS Providence, RI, USA: Dassault Systèmes, 2011, 28.1.1-3-28.1.1-5.

[40] A. Mahmoudi, C. Aird, C. Truman, A. Mirzaee-Sisan, and D. Smith, Generating well defined residual stresses in laboratory specimens, in *ASME 2006 Pressure Vessels and Piping/ICPVT-11 Conference*, (2006) American Society of Mechanical Engineers, 631-639.